

Philipp Grohn<sup>1,\*</sup>  
Dominik Weis<sup>1</sup>  
Markus Thommes<sup>2</sup>  
Stefan Heinrich<sup>3</sup>  
Sergiy Antonyuk<sup>1</sup>


# Contact Behavior of Microcrystalline Cellulose Pellets Depending on their Water Content

Microcrystalline cellulose pellets for oral drug delivery are often produced by a combined wet extrusion-spheronization process. During the entire process, the cylindrical as well as the spherical pellets are exposed to various stresses resulting in a change of their shape and size due to plastic deformation and breakage. In this work, the effect of moisture content of pellets on their mechanical behavior is studied. In static compression tests, the strong influence of water content on deformation behavior of pellets is confirmed. Moreover, impact tests are performed using a setup consisting of three high-speed cameras to record pellet-wall collisions. Material properties, such as stiffness, restitution coefficient, breakage force, and displacement, were analyzed depending on the water content.

**Keywords:** Compression test, Extrusion, Microcrystalline cellulose pellets, Spheronization, Water content

*Received:* September 22, 2019; *revised:* February 28, 2020; *accepted:* March 10, 2020

**DOI:** 10.1002/ceat.201900517

 This is an open access article under the terms of the Creative Commons Attribution License, which permits use, distribution and reproduction in any medium, provided the original work is properly cited.

## 1 Introduction

In agglomeration technology, cylindrical pellets are commonly produced by extrusion or press agglomeration [1]. Especially in the pharmaceutical industry, microcrystalline cellulose (MCC)-based pellets, which are filled into capsules or compressed to multiparticulate tablets, are mainly produced by wet extrusion and subsequent rounding in a spheronization process to achieve an equal, spherical pellet shape [2]. During spheronization, the cylindrical pellets undergo breakage, plastic deformation, and attrition, leading to the desired shape change [3]. On the other hand, in the downstream drying and coating processes, the deformation and breakage of wet pellets has to be avoided to reduce the change of their shape. In any case, the knowledge of the mechanical properties, the deformation and collision behavior of pellets is crucial.

The moisture content of the pellets or saturation degree of their pores plays a dominant role in the nature of their deformation and collision behavior as described in numerous studies. The deformation and breakage mechanisms of wet pellets are strongly influenced by the stress state (static or dynamic, load direction) and loading history (single or multiple cyclic).

For the case of static loading, Schubert [4] investigated the influence of the degree of saturation of wet particulate systems. He found that the strength of pellets strongly depends on their hydro-textural state. Thus, the highest strength of wet pellets is achieved in the so-called capillary state at a degree of saturation of about 0.9, where all pores are nearly filled with liquid (see more in the next section). Pepin et al. [5] reported that the interparticle friction in the contact between the primary particles of wet pellets has a dominant effect on the yield strength.

However, this result is only valid if the dynamic effects during the loading are negligibly small.

At a dynamic stress state, the energy dissipation based on viscous effects due to a high shear flow of the liquid can be dominant. This case occurs typically at the high stress rates and can be significant by high viscous liquids distributed inside the porous structure or in the liquid bridges as well as in the form of layers on the surface of particles [6–11]. Different effects that lead to an increase in energy dissipation for wet pellets are described in the literature [12]. During the approaching of two colliding wet granules, liquid is squeezed out from the pores between primary particles as well as from the contact zone between granules. In addition, a liquid bridge may arise during rebound of the granules. Adams et al. [13] measured the collision behavior of wet granules. They found that at least 97% of the kinetic impact energy is dissipated by viscous effects due to the liquid bridge, which is generated in the contact region for small impact velocities and by bulk viscoplastic effects at higher speeds.

<sup>1</sup>Philipp Grohn, Dominik Weis, Prof. Dr.-Ing. Sergiy Antonyuk  
philipp.grohn@mv.uni-kl.de  
TU Kaiserslautern, Institute of Particle Process Engineering, Gottlieb-Daimler-Strasse 44, 67663 Kaiserslautern, Germany.

<sup>2</sup>Prof. Dr. Markus Thommes  
TU Dortmund University, Laboratory of Solids Process Engineering, Emil-Figge-Strasse 68, 44227 Dortmund, Germany.

<sup>3</sup>Prof. Dr.-Ing. Stefan Heinrich  
Hamburg University of Technology, Institute of Solids Process Engineering and Particle Technology, Denickestrasse 15 (K), 21073 Hamburg, Germany.

The strength of the wet pellets, which show viscoplastic behavior after the yield point caused by the viscous forces, is described in the work of Tardos et al. [14] on the basis of Stokes deformation number which is a ratio of the initial kinetic energy to internal energy resisting deformation. The work of Iveson and Litster [15] reports on a dynamic yield stress of cylindrical wet pellets obtained by extrusion. They showed in the further work [16] that the influence of the viscous forces on the yield strength of the pellets can be related to a capillary number  $Ca$ , which describes the ratio of the viscous force and the surface tension force [17]. Iveson et al. [16] performed compression tests of pellets with different  $Ca$  numbers and found that for  $Ca > 10^{-4}$  the viscous forces will be dominant and significantly influence the yield strength of the wet particles. For this case, the adhesion criteria based on the Stokes number and the “wet” restitution coefficient are used.

The Stokes criterion according to Ennis [10] considers energy dissipation due to viscous effects in the liquid layers on the colliding particles assuming that no plastic deformation is occurring, but a part of kinetic impact energy can dissipate due to an inelastic contact deformation. Liu et al. [12] extended this criterion for the case of the plastic contact deformation. Davis et al. [11] developed a correlation between the so-called “wet” restitution coefficient, which describes the energy dissipation at the collision of wet particles, and the ratio of the Stokes number to its critical value as well as “dry” restitution coefficient, which considers the energy dissipation only due to contact deformation of particles.

To advance the understanding of the strength of wet pellets, this paper focuses on the deformation behavior of pellets with varying water content with respect to the extrusion and spheronization processes. MCC pellets after each process step are tested and the contact behavior is investigated. Single pellet compression tests are conducted for the cylindrical pellets as well as for the spherical pellets. The water content of the pellets is varied, resulting in different deformation behavior from dominantly soft and plastic to stiff elastic. In addition, the restitution coefficient of the pellets is measured with a self-developed setup consisting of three high-speed cameras.

## 2 Theory

### 2.1 Strength of Wet Pellets

Agglomerates or pellets produced by wet extrusion are three-phase systems consisting of a dispersed solid and two immiscible fluid phases. As described in Sect. 1, Schubert [4] investigated such systems using limestone with different water content. Besides, the porosity  $\epsilon_A$ <sup>1)</sup> and the water content  $w$ , the degree of saturation  $S$  are typically used to characterize the hydro-textural state:

$$w = \frac{V_w \rho_w}{V_s \rho_s} \quad (1)$$

1) List of symbols at the end of the paper.

$$\epsilon_A = \frac{V - V_s}{V} \quad (2)$$

$$S = \frac{V_w}{V - V_s} \quad (3)$$

where  $V$  is the overall pellet volume, and  $V_w$  and  $V_s$  are the volumes of the water and solid phases, respectively;  $\rho_w$  and  $\rho_s$  denote the densities of the water and solid phase. The degree of saturation indicates the ratio of the water volume and the overall pore volume. For  $S = 0$ , no liquid is present, at  $S = 1$  the entire pore volume is filled with water. Generally, three main ranges of saturation degree of hydrophobic primary particles are differentiated according to Schubert [4] (Fig. 1).

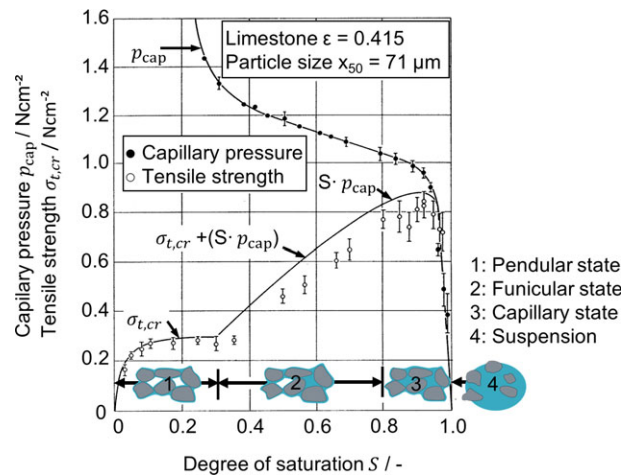


Figure 1. Tensile strength and capillary pressure as a function of degree of saturation according to Schubert [4].

The pendular state is referred to a degree of saturation of  $S \leq 0.3$ , since at a sufficiently small amount of water content in the pellet individual liquid bridges are formed between the primary particles. Increasing the liquid content above  $S = 0.3$  leads to a funicular state, where liquid bridges and pores filled with liquid can coexist. From a saturation value of  $S \geq 0.8$ , the pores are mostly filled with liquid. In this so-called capillary state, the capillary negative pressure in the agglomerate is the strength-determining factor.

Under the assumption that the liquid is evenly distributed in the agglomerate, Schubert has developed the following equation for the maximum tensile strength in the capillary state [18]:

$$\sigma_{t,cr} = Sp_{cap} = S\alpha\gamma_{la} \cos \delta \frac{1}{d_{32}} \frac{1 - \epsilon_A}{\epsilon_A} \quad (4)$$

where  $p_{cap}$  is the capillary pressure, which is calculated from the surface tension  $\gamma_{la}$ , the wetting angle  $\delta$ , Sauter diameter  $d_{32}$ , the porosity of the agglomerate  $\epsilon_A$ , and a correction factor  $\alpha$ . For monomodal spherical primary particles,  $\alpha$  can be assumed to be 6, for irregularly shaped primary particles 8. If the degree of saturation becomes larger than 1, a coating on full saturated particles or a droplet containing the particles are formed [4, 19].

## 2.2 Extrusion and Spheronization

As described in the introduction, the spherical pellets were produced from the extrudates in a subsequent spheronization process. Fig. 2 demonstrates the typical change of the hydro-textural state of the pellets during extrusion and spheronization according to Galland et al. [20]. In the first step, the wet mass (2) is prepared. Different types of granulators are used for the mixing of the powders (1) and the granulation liquid [21]. The granulation can also be carried out in the first zone of the extrusion process. It can be seen that the extrusion of the wet mass (2) results in an increase of the saturation degree and a decrease of the porosity while the water content remains constant. Thus, in the extrusion step a total drainage of the gas phase is possible, resulting in nearly biphasic (solid/liquid) extrudates (3b) [22].

During spheronization, the hydrotextral state of the pellets remains constant if the saturation degree of 1 was reached in the extrusion step. In this case, only the pellet shape changes. However, if the saturation of the extrudates is not reached during the extrusion step (3a), the porosity and the saturation degree might vary [20]. After spheronization, the resulting wet pellets have a saturation of 1 (3b). In a final step, the spheronized pellets can be dried, leading to a lower porosity and water content.

## 2.3 Coefficient of Restitution

The coefficient of restitution ( $COR$ ) is a parameter describing the impact behavior during dynamic loading.  $COR$  is defined as the ratio of the rebound velocity and the initial velocity between two bodies after their collision [23, 24]. It describes the energy dissipation  $E_{diss}$  during the impact of two bodies by the ratio of the kinetic energy after  $E_{kin,R}$  to before the impact  $E_{kin}$ :

$$COR = \sqrt{\frac{E_{kin,R}}{E_{kin}}} = \sqrt{1 - \frac{E_{diss}}{E_{kin}}} \quad (5)$$

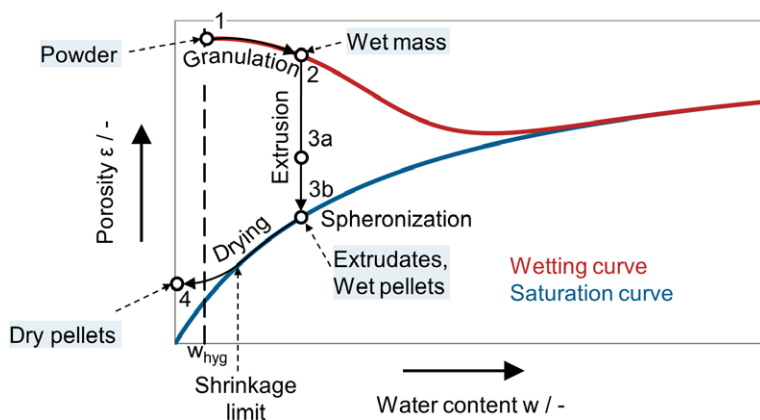


**Figure 2.** Typical change of the hydro-textural state of the pellets during extrusion and spheronization according to Galland [20].

Assuming that there is no mass loss due to attrition or breakage during impact, the following impression can be made for  $COR$ :

$$COR = \frac{|\vec{v}_R|}{|\vec{v}|} \quad (6)$$

where  $v_R$  is the velocity after the rebound and  $v$  the velocity before the impact.  $COR$  ranges from 0 for an entirely plastic collision up to 1 in the case of a perfect elastic behavior. While no kinetic energy is dissipated for a  $COR$  of 1, the entire energy is converted to heat or dissipated due to viscous or to plastic deformation for a  $COR$  of 0.

## 3 Experimental Setups and Material

### 3.1 Compression Test

The experimental setup for the compression tests is displayed in Fig. 3. For the experimental investigation of the deformation behavior of the pellets, a Texture Analyser® (TA.XTplus, Stable Micro Systems) was used. In order to examine the influence of the water content, the compression tests were carried out in a climatic chamber at a relative humidity of 90–95 % to prevent the pellets from drying. Thus, the pellet, the compression plate, and the punch were located within the climatic chamber. As a result, the measured water content of the pellets at the beginning and at the end of the compression tests remained constant. The water content of the MCC pellets before each test series was determined with a MA100 Moisture Analyzer (Sartorius, Goettingen, Germany).

In order to capture the dimensions of each pellet, images of the pellet were taken immediately before the compression tests. For taking the images, the pellets were placed on a black surface with a scale inside the climate chamber and photographed with a camera (1334×750 pixels, 326 ppi). The images were transferred to a binary image and evaluated by using the MATLAB Image Processing Toolbox. Thus, the diameter, length, sphericity, and aspect ratio of the pellets were calculated by determining the number of pixels in the length and width of each pellet.

The pellets with different water content were uniaxially loaded with a velocity of  $0.02 \text{ mm s}^{-1}$ . Tests were performed until breakage occurred. In addition, loading-unloading and cyclic loading tests without breakage were carried out.

### 3.2 Setup for 3D High-Speed Capturing of Pellet-Wall Impact (Coefficient of Restitution)

The dynamic loading was studied using a setup consisting of two synchronized high-speed cameras (camera 1 and 2; IDT Os7) to record the pellet-wall collision three-dimensionally (Fig. 4). In addition, a third high-speed camera (camera 3; IDT Y8) equipped with a 12.5× distance microscope lens (MacroLens) was employed in order to resolve the

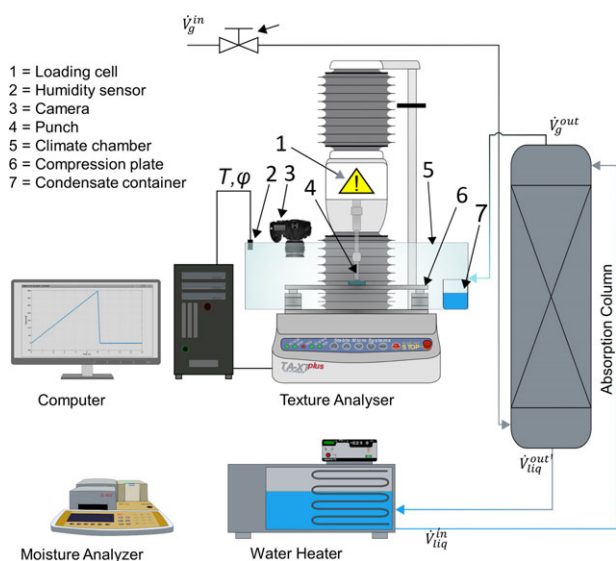


Figure 3. Experimental setup for the compression tests.

contact between the surface and the pellet. This setup was developed in order to measure the restitution coefficient of small particles down to a size of  $30\ \mu\text{m}$  and non-spherical pellets [24]. With the cameras, aligned in an angle of  $90^\circ$  relative to each other, it is possible to record the trajectory, the rotation, and the rebound angle of the pellet during the free fall tests. This is particularly important for cylindrical pellets, as different contact scenarios, depending on the contact angle  $\theta$ , have to be considered (Fig. 4).

For the exposure, two LED light sources (Constellation 120E) were used. The cylindrical pellets were vertically fixed on the vacuum nozzle and dropped on a flat surface with an impact velocity of about  $2\ \text{m s}^{-1}$  (Fig. 4). Using a motion trigger, the pellet impact was recorded simultaneously by the cameras with a frame rate of 6000 fps and a resolution of  $1024 \times 460\ \text{px}$ .

In order to determine the COR, 100 frames before and after the impact were processed by a MATLAB script using the Image Processing Toolbox. The images were transferred to a binary image. For every image, the area center of the pellet was calculated and thus the pellet position during collision could be tracked. Knowing the scale factor and the frame rate of the cameras, the exact pellet velocity before and after the impact could be determined and the coefficient of restitution was calculated by Eq. (6).

### 3.3 Materials

The pellets in this study were produced by the extrusion and spheronization process. An amount of  $2\ \text{kg h}^{-1}$  of a powder mixture consisting of a mass fraction of microcrystalline cellulose (Vivapur 102, JRS Pharma, Germany) of  $w_i = 0.2\ \text{g g}^{-1}$  and a mass fraction of  $\alpha$ -lactose monohydrate (Granulac 200, Meggle, Germany) of  $w_i = 0.8\ \text{g g}^{-1}$  were extruded in an extruder (Micro 27 GL-28D, Leistritz, Germany) with 100 rpm under dosage of conserved water ( $0.8\ \text{kg h}^{-1}$ ). The extrudates were then spheronized in a laboratory-scale spheronizer (R250, Gabler, Germany) with a load of 300 g and a rotational speed of the friction disk of 750 rpm for 5 min. The resulting MCC pellets before and after the spheronization process are depicted in Fig. 5.

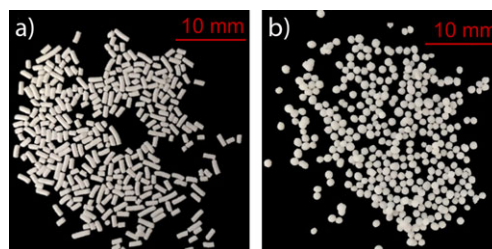


Figure 5. Wet cylindrical pellets (a) after extrusion and (b) after spheronization.

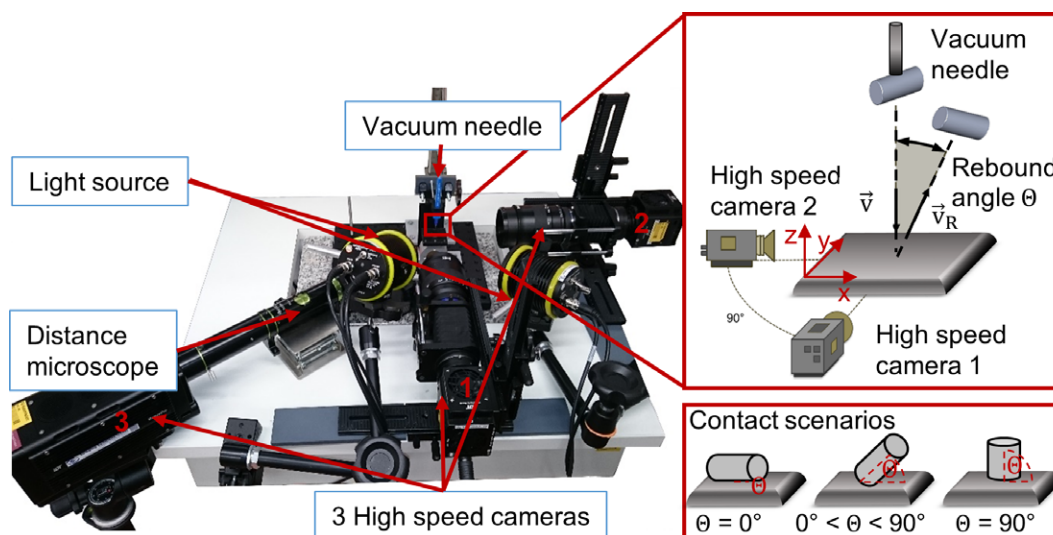


Figure 4. Setup for measurement of the restitution coefficient of cylindrical pellets and possible contact scenarios of the cylindrical pellet with the surface.

The water content of the pellets after the extrusion and after the spheronization step was found to be 37.2%. In order to investigate the influence of the water content of the MCC pellets on their deformation behavior, the wet pellets were dried for variable time intervals at ambient air (19 °C). The final water content of the pellets could thus varied from 37.2% to 1.3% after 24 h of drying (Tab. 1).

**Table 1.** Drying time and water content of the pellets.

Drying time [min]	Water content [%]
0	37.17
10	32.70
20	19.46
32	10.75
65	5.49
75	3.56
> 24 h	1.33

The pellet dimensions were obtained by the image analysis procedure described in Sect. 3.1, which was applied in total to 700 cylindrical and 500 spherical pellets. The mean length and standard deviation of the extrudates was found to be  $2.23 \pm 0.41$  mm while the diameter was  $1.06 \pm 0.06$  mm. For the spherical pellets a diameter of  $1.21 \pm 0.09$  mm was measured.

## 4 Results

### 4.1 Compression Tests of Pellets with Different Water Contents and Shapes

During the process of extrusion and spheronization, the pellets change their shape and hydro-textural state. To capture the mechanical properties of the pellets after the different process steps, cylindrical as well as spherical pellets with different water contents were investigated, respectively.

In Fig. 6, typical force-displacement curves of a cylindrical pellet with a water content of 37.2% (Fig. 6a) and with a water

content of 1.3% (Fig. 6b) are presented. Since the extrudates do not have an ideal cylindrical shape, the diameter varies over the length. For this reason, the pellets were not in contact with the compression plate over the entire length at the beginning of the compression. Therefore, the force-displacement curve is non-linear at the beginning of the measurements. This effect is smaller for pellets with higher water content, as they are softer and deform more plastic.

The slope in the range of the linear increase of the force-displacement curve before the primary breakage occurs (Point A in Fig. 6) corresponds to the stiffness of the pellet. It can be seen that the slope of the graph for the dry pellet is much higher, which means that the pellet is significantly stiffer than the wet pellet. For the wet pellet breakage occurred at a force of 0.13 N, while the breakage force of the dry pellet was much higher. In the present case, the required breakage force was 2.4 N.

In Fig. 7, the images of the tested MCC pellets before and after compression until breakage are displayed. Although the initial sizes of the pellets were similar, the wet pellet showed a failure strain of 10.1% while breakage occurred at a strain of 4.6% for the dry pellet. Thus, the deformation until breakage for the wet pellet is more than twice as high. As demonstrated, e.g., in [25], a more brittle breakage (the cracks extend unsteady) led to a higher drop in the force displacement curve. In the force-displacement curve for the wet pellet, no decrease in force is observed, which is an indication of a ductile fracture. The curve for the dry pellets shows a significant decrease in force, which is more indicative of an elastic-plastic fracture. If the punch continues to load the wet pellet after primary breakage, the broken fragments of the pellet are further deformed and therefore the curve increases again. In the case of the dry pellets, further secondary breakage is observed (Points B, C, D in Fig. 6).

The results of the compression tests till primary breakage of the spherical and cylindrical pellets with different water contents are presented in Fig. 8. For each data point, 100 pellets were examined by compression tests. In Fig. 8a, the measured stiffness is plotted versus the water content of the pellets. It is obvious that the stiffness of the pellets with low water content is significantly higher than that of cylindrical pellets with higher water content. Fig. 8b indicates the breakage displacement as a function of the water content of the pellets. Due to a more plastic deformation behavior of the wet pellets, the deformation of the pellets before breakage is higher. In Fig. 8c, the breakage force is plotted versus the water content of the pellets. It can be seen that pellets with low water content require a higher force for breakage than pellets with higher water content. The performed compression tests correspond to a  $Ca$  number of  $2.74 \times 10^{-7}$ , therefore, the viscous effects can be neglected.

According to Galland [22], the degree of saturation of the extrudates during the extrusion can reach values close to 1 (see Fig. 2). At this high degree of saturation the pellets can be assigned to the capillary state according to Schubert [4]. In this case, the pores are mainly filled with water and the strength is determined by the capillary pressure.

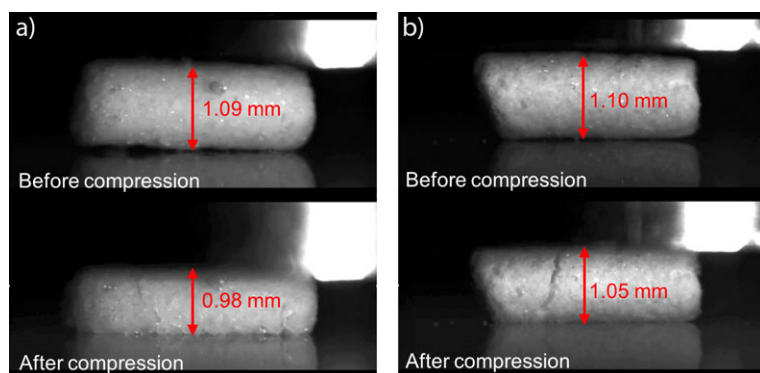


**Figure 6.** Typical force-displacement curves for (a) the wet MCC pellet and (b) the dry MCC pellet during the uniaxial compression.

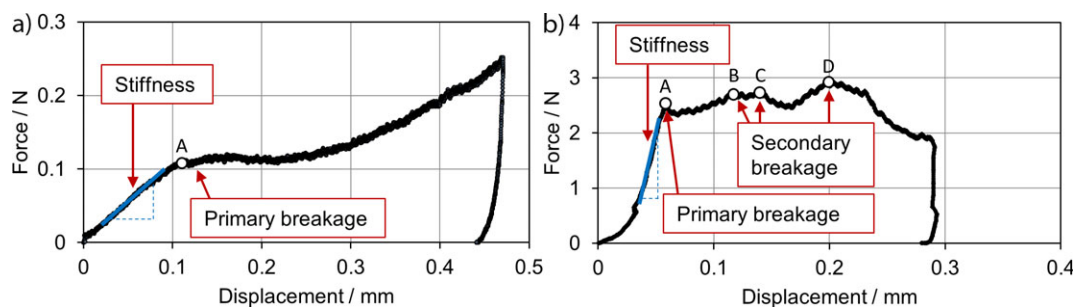


**Figure 7.** Images of an MCC pellet with a water content of (a) 37.2 % and (b) 1.3 % before and after the compression test obtained by a high-speed camera.

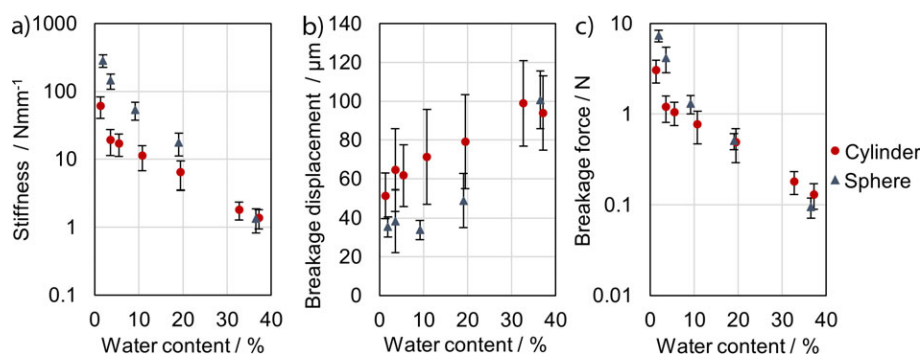


**Figure 8.** Influence of the water content of cylindrical and spherical MCC pellets on (a) the stiffness, (b) the breakage displacement, and (c) the breakage force.

reason, the strength of the pellet increases with decreasing water content. It can be assumed that during the spheronization process the distribution of the primary particles in the pellets becomes more homogeneous. Therefore, more interparticle contacts are created which lead to an increasing number of solid bridges during drying of the spheronized pellets compared to the extrudates. This effect could explain the higher stiffness and breakage force of spherical pellets with water contents less than 20 %.

Galland [22] showed that the water content is the same for wet extrudates and wet spheronized pellets. Assuming that the extrudates are saturated, also the porosity does not change during spheronization. Therefore, the hydro-textural state of the pellets does not change during pellet rounding, which explains that there is no significant difference in the deformation and breakage behavior for wet cylindrical and spherical pellets with water contents higher than 20 %.

However, the measured breakage forces are in a critical region regarding stresses occurring in a spheronization process. In our previous work [26], the forces acting on cylindrical as well as spherical MCC pellets with a water content of 37.2 % during the spheronization process were obtained by simulation. Due to the different mass and shape of the extrudates compared to the spherical pellets, different average values of the collision force were obtained, namely, 0.13 N for the cylindrical extrudates and 0.06 N for the spherical pellets. The comparison with the breakage forces measured in this study for the wet pellets indicates that the forces, which act on the spherical pellets during spheronization, should not lead to pellet breakage. On the other hand, the forces acting on the cylindrical pellets are in the critical region regarding pellet breakage. Therefore, only for the cylindrical pellets breakage can occur during spheronization while the spherical pellets remain stable.

During the drying process, the water content decreases and solid bridges are formed between primary particles. These solid bridges are more stable than the capillary bridges. For this

## 4.2 Cyclic Loading of the Cylindrical Pellets

During the spheronization process, the cylindrical MCC pellets are subjected to repeated stressing in order to achieve the desired rounding. The influence of cyclic loading and unloading on the deformation behavior of the cylindrical pellets was examined. In Fig. 9, the force-displacement curves for a cyclic loading-unloading test of a pellet with 37.2 % water content are displayed. In each cycle, the pellet was loaded to a force of 75 % of the average breakage force obtained by the experiments in

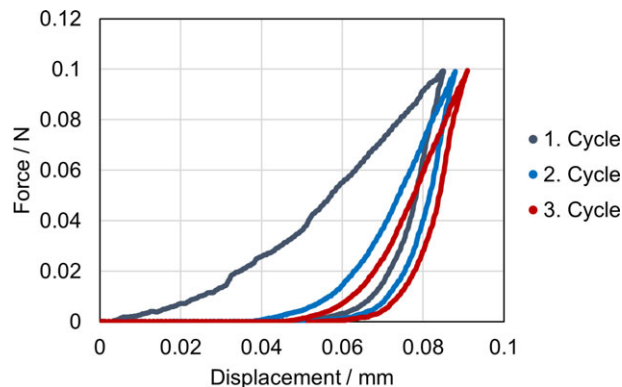


**Figure 9.** Force-displacement diagram for a cyclic loading-unloading test of a wet MCC pellet (37.2 % water content).

Sect. 4.1. The plastic strain, which is a ratio of the plastic deformation over the initial diameter of the pellet, could be calculated by determining these data from the measurement. During the first loading-unloading cycle, a plastic strain of 4.4 % was obtained. The plastic strain decreased during further cycles, e.g., in the second cycle a plastic strain of 0.7 % occurred.

In Tab. 2, the plastic strain for 100 pellets with a water content of 37.2 % as well as for 100 pellets with a water content of 1.3 % after each cycle is given. As already shown in Fig. 7, the dry pellets deform not as much as the wet pellets during loading. The average plastic deformation from the first to the second cycle for the dry pellets was 1.9 %. Tab. 2 demonstrates that the plastic strain of dry pellets under cyclic loading is less than half the plastic strain for wet pellets.

In Tab. 2 also the stiffness for the dry and wet pellets is listed. For the wet pellets, the calculated stiffness was determined in the plastic deformation range, which is characterized by an approximately linear slope of the force-displacement curves (Fig. 6). From cycle 1 to 2, there is an increase of 118.5 % for the wet pellets. As can be seen from the force-displacement diagram in Fig. 9, the change from the second to the third cycle is less significant, namely, an increase of 13.4 % for the wet pellets. The dry pellets show a similar behavior, yet the differences are less strong. From the first to the second cycle, there is an increase of 34.2 % for the dry pellets and of 2.22 % from the second to the third cycle. These changes can be attributed to the enlarged contact area due to plastic deformation and to hardening of the material in the contact area.

### 4.3 Measurements of the Coefficient of Restitution

The measurements of COR were performed with the setup described in Sect. 3.2. In order to prevent the pellets from drying during the experiments, the climate chamber was also used. In contrast to spherical pellets, the COR for cylindrical pellets also depends on the contact scenario, which means on the contact angle  $\theta$  between the impact plate and the pellet, as can be seen in Fig. 4. Therefore, the collision of the pellets was recorded by two cameras and the velocities before and after the impact are determined as:

$$v = \sqrt{v_x^2 + v_y^2 + \left(\frac{v_{z,1} + v_{z,2}}{2}\right)^2} \quad (7)$$

**Table 2.** Dependence of the plastic strain and stiffness on the number of cycles for wet and dry MCC pellets.

	Plastic strain (mean $\pm$ std. dev) [%]		Stiffness (mean $\pm$ std. dev) [Nmm <sup>-1</sup> ]	
	Wet pellets <sup>a)</sup>	Dry pellets <sup>b)</sup>	Wet pellets <sup>a)</sup>	Dry pellets <sup>b)</sup>
Cycle 1	4.40 $\pm$ 0.14	1.86 $\pm$ 0.39	1.39 $\pm$ 0.23	17.76 $\pm$ 1.63
Cycle 2	0.69 $\pm$ 0.14	0.19 $\pm$ 0.09	3.04 $\pm$ 0.25	23.83 $\pm$ 0.84
Cycle 3	0.28 $\pm$ 0.19	0.13 $\pm$ 0.05	3.44 $\pm$ 0.27	24.36 $\pm$ 0.64

<sup>a)</sup>37.2 % water content; <sup>b)</sup>1.3 % water content

Where  $v_x$  is the captured velocity in horizontal direction from camera 1,  $v_y$  is the velocity in horizontal direction from camera 2, and  $v_{z,i}$  is the velocity in vertical direction from each camera. In Fig. 4, the location of the coordinate system is indicated. The restitution coefficient is then calculated by the ratio of the velocity after to before the impact (Eq. (6)). Caused by different rotational movements of the cylindrical pellets during acceleration, they hit the plate with different contact angles. The COR for the wet cylindrical pellets could not be determined, because breakage occurred. Apart from the wet cylindrical pellets, the other pellets tested showed no breakage and thus no loss of mass; therefore, the COR could be calculated by the impact and rebound velocities.

In Tab. 3, the average values of COR are given calculated based on 100 repeated free-fall tests, respectively. As in the compression tests, the wet pellets had a water content of 37.2 % and the water content of the dry pellets was 1.3 %. In comparison with the quasi-static compression tests, the energy dissipation because of vicious shear flow is much higher due to the capillary effects because of the higher *Ca* number of 0.027. The wet pellets exhibit a much more plastic behavior during impact than the dry pellets, resulting in the distinct decrease of the COR. In the case of cylindrical pellets, a part of the impact energy is transferred into rotational energy during rebound.

**Table 3.** Measured restitution coefficient (COR) of MCC pellets during dynamic impact.

	COR (mean $\pm$ std. dev)
Dry spherical pellet	0.664 $\pm$ 0.057
Wet spherical pellet	0.110 $\pm$ 0.058
Dry cylindrical pellet	0.422 $\pm$ 0.194

The first contact of the cylindrical pellet with the wall was usually observed with one end of the pellet. As a result, the pellet starts to rotate during the rebound. It was observed that the pellet rotates mainly around its center of gravity. Therefore, the measured COR is generally lower compared to spherical dry pellets. In addition, the different contact scenarios also have an influence on the energy dissipation during the dynamic impact. Depending on the angle of impact, the contact area is different and due to an uneven pellet surface, several contact points can occur during the impact. As a consequence, the standard deviation of cylindrical pellets is much higher compared to the spherical ones.

## 5 Conclusion

The deformation behavior of spherical and cylindrical MCC pellets with different water contents were experimentally investigated by compression and impact tests. The uniaxial compression tests showed a high dependence of the deformation behavior on the water content of the MCC pellets. The obtained results indicate that the stiffness and

breakage force of the pellets increase with the decreasing water content. At low water content, the spherical pellets require a higher force for breakage than the extrudates; however, at water contents higher than 20 % no difference can be observed.

During the drying process, the water content decreases and solid bridges are formed between primary particles. These solid bridges are more stable than the capillary bridges. It can be assumed that during the spheronization process more interparticle contacts are created which lead to an increasing number of solid bridges. This effect could explain the higher strength of the dry spherical pellets.

The degree of saturation of the extrudates during the extrusion can reach values close to 1. Assuming that the extrudates are saturated, also the porosity does not change during spheronization. Therefore, the hydro-textural state of the wet pellets does not change during pellet rounding, which explains that there is no difference in the deformation behavior for the cylindrical and spherical pellets with water contents higher than 20 %.

The measured average breakage forces were compared with simulation results of the spheronization process with cylindrical and spherical pellets. It could be shown that the average breakage force is not reached for the spherical pellets, but for the cylindrical ones. Thus, breakage is expected for the cylindrical extrudates while the spherical pellets do not break.

The analysis of the force-displacement curves obtained by cyclic loading-unloading tests showed a more plastic behavior of the material with higher water content. With an increasing number of cycles the residual displacement decreases. Consequently, the contact stiffness of the particles increases with the number of cycles. These changes indicate that the repeated mechanical stress leads to a larger contact area and resistance of the material against deformation in the contact area.

The dry spherical pellets have the highest coefficient of restitution, whereas the wet spherical pellets have a value close to 0 due to their high plastic deformation behavior. The *COR* of the wet cylindrical pellets could not be measured since parts of the pellets break off at impact. Compared to the dry spherical pellets, the *COR* of the dry cylindrical pellets is lower. During the rebound, a part of the kinetic energy is converted into rotational energy. Additionally, the different contact scenarios of the pellet with the surface have to be considered. Depending on the angle of impact, the contact surface varies. Moreover, several contacts can occur during impact due to the uneven pellet surface. This influences the energy dissipation during the impact.

The findings of this study can improve the accuracy of simulation models in the prediction of the deformation and breakage processes in spheronization of MCC pellets. The obtained mechanical properties are essential parameters of the contact models in the numerical simulation with the discrete element method. Moreover, the results of this study can help to derive meaningful data from simulation results.

## Acknowledgment

This study was conducted within two research projects funded by the Deutsche Forschungsgemeinschaft (DFG, German

Research Foundation), Project-ID AN 782/12-1 and AN 782/2-1, which is gratefully acknowledged.

*The authors have declared no conflict of interest.*

## Symbols used

<i>COR</i>	[-]	coefficient of restitution
$d_{32}$	[m]	Sauter diameter
$E_{\text{diss}}$	[J]	dissipated energy
$E_{\text{kin}}$	[J]	kinetic impact energy
$E_{\text{kin,R}}$	[J]	kinetic rebound energy
$p_{\text{cap}}$	[N cm <sup>-2</sup> ]	capillary pressure
<i>S</i>	[-]	degree of saturation
$v_{\text{R}}$	[m s <sup>-2</sup> ]	velocity of the rebound
$v$	[m s <sup>-2</sup> ]	velocity of the impact
<i>V</i>	[m <sup>3</sup> ]	overall pellet volume
$V_{\text{L}}$	[m <sup>3</sup> ]	volume liquid phase
$V_{\text{S}}$	[m <sup>3</sup> ]	volume solid phases
<i>w</i>	[%]	water content

## Greek letters

$\alpha$	[-]	correction factor
$\gamma_{\text{la}}$	[N m <sup>-1</sup> ]	surface tension
$\delta$	[°]	wetting angle
$\varepsilon_{\text{A}}$	[-]	porosity of an agglomerate
$\theta$	[°]	contact angle between impact plate and pellet
$\rho_{\text{L}}$	[kg m <sup>-3</sup> ]	density liquid
$\rho_{\text{S}}$	[kg m <sup>-3</sup> ]	density solid
$\sigma$	[N cm <sup>-2</sup> ]	tensile strength

## Abbreviations

MCC microcrystalline cellulose

## References

- [1] W. Pietsch, *Agglomeration in Industry: Occurrence and applications*, Wiley-VCH, Weinheim 2005.
- [2] S. Muley, T. Nandgude, S. Poddar, *Asian J. Pharm. Sci.* **2016**, *11* (6), 684–699. DOI: <https://doi.org/10.1016/j.ajps.2016.08.001>
- [3] D. Weis, M. Niesing, M. Thommes, S. Antonyuk, *Chem. Ing. Tech.* **2017**, *89* (8), 1083–1091. DOI: <https://doi.org/10.1002/cite.201600154>
- [4] H. Schubert, *Powder Technol.* **1984**, *37* (1), 105–116. DOI: [https://doi.org/10.1016/0032-5910\(84\)80010-8](https://doi.org/10.1016/0032-5910(84)80010-8)
- [5] X. Pepin, S. J. R. Simons, S. Blanchon, D. Rossetti, G. Couaraze, *Powder Technol.* **2001**, *117* (1–2), 123–138. DOI: [https://doi.org/10.1016/S0032-5910\(01\)00324-2](https://doi.org/10.1016/S0032-5910(01)00324-2)
- [6] B. Crüger, S. Heinrich, S. Antonyuk, N. G. Deen, J. A. M. Kuipers, *Chem. Eng. Res. Des.* **2016**, *110*, 209–219. DOI: <https://doi.org/10.1016/j.cherd.2016.01.024>
- [7] S. Antonyuk, S. Heinrich, N. Deen, H. Kuipers, *Particuology* **2009**, *7* (4), 245–259. DOI: <https://doi.org/10.1016/j.partic.2009.04.006>



- [8] O. Pitois, P. Moucheront, X. Chateau, *J. Colloid Interface Sci.* **2000**, *231* (1), 26–31. DOI: <https://doi.org/10.1006/jcis.2000.7096>
- [9] D. Rossetti, X. Pepin, S. J. R. Simons, *J. Colloid Interface Sci.* **2003**, *261* (1), 161–169. DOI: [https://doi.org/10.1016/S0021-9797\(03\)00043-2](https://doi.org/10.1016/S0021-9797(03)00043-2)
- [10] B. J. Ennis, G. Tardos, R. Pfeffer, *Powder Technol.* **1991**, *65* (1–3), 257–272. DOI: [https://doi.org/10.1016/0032-5910\(91\)80189-P](https://doi.org/10.1016/0032-5910(91)80189-P)
- [11] R. H. Davis, D. A. Rager, B. T. Good, *J. Fluid Mech.* **2002**, *468*, 107–119. DOI: <https://doi.org/10.1017/S0022112002001489>
- [12] L. X. Liu, J. D. Litster, S. M. Iveson, B. J. Ennis, *AIChE J.* **2000**, *46* (3), 529–539. DOI: <https://doi.org/10.1002/aic.690460312>
- [13] J. Fu, M. J. Adams, G. K. Reynolds, A. D. Salman, M. J. Hounslow, *Powder Technol.* **2004**, *140* (3), 248–257. DOI: <https://doi.org/10.1016/j.powtec.2004.01.012>
- [14] G. I. Tardos, M. I. Khan, P. R. Mort, *Powder Technol.* **1997**, *94* (3), 245–258. DOI: [https://doi.org/10.1016/S0032-5910\(97\)03321-4](https://doi.org/10.1016/S0032-5910(97)03321-4)
- [15] S. M. Iveson, J. D. Litster, *Powder Technol.* **1998**, *99* (3), 234–242. DOI: [https://doi.org/10.1016/S0032-5910\(98\)00115-6](https://doi.org/10.1016/S0032-5910(98)00115-6)
- [16] S. M. Iveson, J. A. Beathe, N. W. Page, *Powder Technol.* **2002**, *127* (2), 149–161. DOI: [https://doi.org/10.1016/S0032-5910\(02\)00118-3](https://doi.org/10.1016/S0032-5910(02)00118-3)
- [17] S. J. R. Simons, X. Pepin, D. Rossetti, *Int. J. Miner. Process.* **2003**, *72* (1–4), 463–475. DOI: [https://doi.org/10.1016/S0301-7516\(03\)00120-0](https://doi.org/10.1016/S0301-7516(03)00120-0)
- [18] H. Schubert, *Kapillarität in porösen Feststoffsystemen (Capillarity in Porous Solid Material Systems)*, Springer-Verlag, Berlin **1982**.
- [19] H. Rumpf, *Mechanische Verfahrenstechnik*, Hanser, München **1975**.
- [20] S. Galland, T. Ruiz, M. Delalonde, A. Krupa, B. Bataille, *Powder Technol.* **2005**, *157* (1–3), 156–162. DOI: <https://doi.org/10.1016/j.powtec.2005.05.037>
- [21] R. Gandhi, C. Lal Kaul, R. Panchagnula, *Pharm.Sci. Technol. Today* **1999**, *2* (4), 160–170. DOI: [https://doi.org/10.1016/S1461-5347\(99\)00136-4](https://doi.org/10.1016/S1461-5347(99)00136-4)
- [22] S. Galland, T. Ruiz, M. Delalonde, *Int. J. Pharm.* **2007**, *337* (1–2), 239–245. DOI: <https://doi.org/10.1016/j.ijpharm.2007.01.011>
- [23] S. Antonyuk, S. Heinrich, J. Tomas, N. G. Deen, M. S. van Buijtenen, J. A. M. Kuipers, *Granular Matter* **2010**, *12* (1), 15–47. DOI: <https://doi.org/10.1007/s10035-009-0161-3>
- [24] F. Krull, R. Hesse, P. Breuninger, S. Antonyuk, *Chem. Eng. Res. Des.* **2018**, *135*, 175–184. DOI: <https://doi.org/10.1016/j.cherd.2018.05.033>
- [25] A. Carpinteri, F. Cardone, G. Lacidogna, *Strain* **2009**, *45* (4), 332–339. DOI: <https://doi.org/10.1111/j.1475-1305.2008.00615.x>
- [26] D. Weis, M. Niesing, M. Thommes, S. Antonyuk, *EPJ Web Conf.* **2017**, *140*, 15005. DOI: <https://doi.org/10.1051/epjconf/201714015005>